2026 IEEE International Conference on Robotics and Automation (ICRA 2026)
June 1-5, 2026. Vienna, Austria

Flexible and Foldable: Workspace Analysis and Object Manipulation Using a Soft, Interconnected, Origami-Inspired Actuator Array

Bailey Dacre[1], Rodrigo Moreno[1], Serhat Demirtas[2], Ziqiao Wang[2], Yuhao Jiang[2], Jamie Paik[2], Kasper Stoy[1], Andrés Faíña[1]

***Abstract*— Object manipulation is a fundamental challenge in robotics, where systems must balance trade-offs among manipulation capabilities, system complexity, and throughput. Distributed manipulator systems (DMS) use the coordinated motion of actuator arrays to perform complex object manipulation tasks, seeing widespread exploration within the literature and in industry. However, existing DMS designs typically rely on high actuator densities and impose constraints on object-to-actuator scale ratios, limiting their adaptability. We present a novel DMS design utilizing an array of 3-DoF, origami-inspired robotic tiles interconnected by a compliant surface layer. Unlike conventional DMS, our approach enables manipulation not only at the actuator end effectors but also across a flexible surface connecting all actuators; creating a continuous, controllable manipulation surface. We analyse the combined workspace of such a system, derive simple motion primitives, and demonstrate its capabilities to translate simple geometric objects across an array of tiles. By leveraging the inter-tile connective material, our approach significantly reduces actuator density, increasing the area over which an object can be manipulated by approximately $\times 1.84$ without an increase in the number of actuators. This design offers a lower cost and complexity alternative to traditional high-density arrays and introduces new opportunities for manipulation strategies that leverage the flexibility of the interconnected surface.**

Keywords: Soft robot, Distributed Robot Systems, Origami Robot, Object Manipulation, Robotic Workspace

I. Introduction

Object manipulation tasks are commonplace both within the literature and in industry. Systems with few degrees of freedom (DoF), such as conveyors, offer high throughput and payload capacity but are limited in their manipulation capabilities, typically to single-axis translation, lacking the capabilities for rotation or independent object manipulation. In contrast, more dexterous systems like 6-DoF robotic arms provide greater precision and control but at the cost of increased complexity, reduced throughput, and limited parallel manipulation capabilities. Such systems also struggle to handle heterogeneous, irregularly shaped, or soft objects without specialized grippers.

Distributed manipulator systems (DMS) offer an alternative approach to manipulation, able to perform precise, multi-dimensional object manipulation. These systems typically utilize planar arrays of actuators. These actuators — individually limited to few DoF — do not directly grip objects but rely on the coordinated application of force from many actuators to move objects. These systems have been able to perform tasks such as translation, in-plane and out-of-plane rotation via collective actuation. Demonstrated at both the microscopic and macroscopic scales, these actuator arrays offer an appealing alternative to traditional system architectures, offering complex manipulation capabilities, with inbuilt redundancy and high bandwidth afforded by their many cooperating actuators. Actuation mechanisms vary widely, including pistons [1], wheels [2], [3], parallel mechanisms [4], [5], and cilia [6].

In this work, we present an array of 3-DoF origami-inspired parallel mechanism robotic tile actuators, interconnected by a layer of flexible material to form a continuous manipulation surface. Unlike conventional DMS, this architecture enables actuation both at the end effectors and across the deformable surface. This connective material allows for a far lower actuator density than comparable DMS, lowering both the cost and complexity. We analyse the workspace of such a connected multi-actuator system and develop coordinated motion primitives. We demonstrate how the use of continuous compliant surfaces facilitates the manipulation of objects significantly smaller than the inter-actuator spacing, relaxing traditional scale and density constraints, as well as facilitating new manipulation strategies.

The main contributions of this work are as follows.

- Design of a continuous manipulation surface using 3-DoF origami-inspired actuators interconnected through a flexible layer.
- Characterization of the system workspace and demonstration of coordinated motion primitives.
- Experimental validation of the manipulation of diverse object geometries, including objects smaller than the inter-actuator spacing.

II. Related Work

Various designs of DMS have been explored for object manipulation, typically structured as 2D actuator arrays enabling in-plane movement. Some systems, such as piston or wheel based arrays, rely on contact with multiple actuators simultaneously. Few points of contact can provide planar control, but performance degrades when objects are smaller than the inter-actuator spacing. Conversely, systems using micro-scale actuators (such as MEMS oscillators) utilize a high actuator density, approximating programmable vector fields. Although dense arrays of small actuators facilitate the manipulation of objects of varied size and geometry, control

[1]REAL Lab, IT University of Copenhagen (ITU), Denmark. Emails: {baid, rodr, ksty, anfv}@itu.dk
[2]Reconfigurable Robotics Lab (RRL), EPFL, Switzerland. Emails: {serhat.demirtas, ziqiao.wang, yuhao.jiang, jamie.paik}@epfl.ch

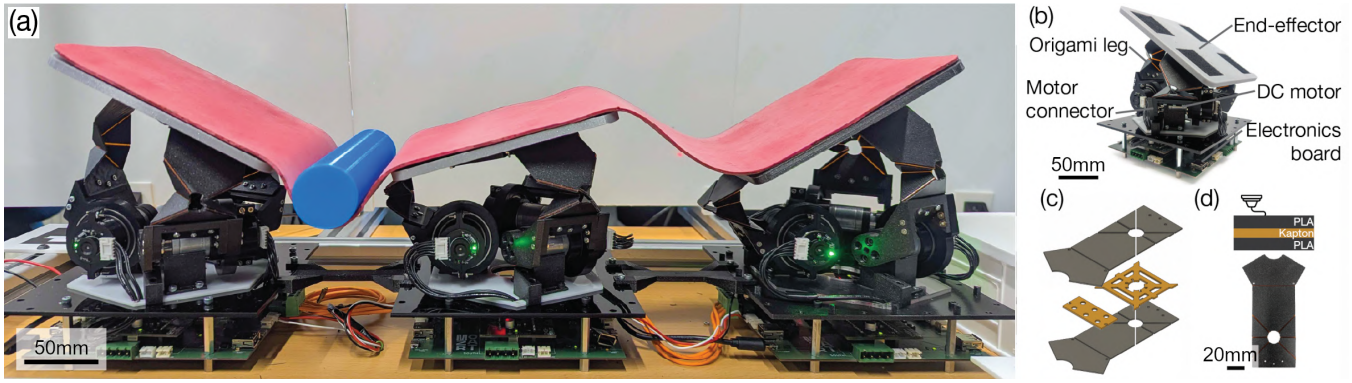

Fig. 1: Overview of the robotic surface manipulation system and its components. (a) Actuator array of 3 robotic tiles with an inter-tile distance $D = 240\,mm$ and $L = 100\,mm$ manipulating a cylinder. (b) A robotic tile module with three origami legs and attachment points for the flexible surface on its end effector. (c) Exploded view of origami leg. (d) Fabricated origami leg composed of $0.127\,mm$ polyimide embedded within $1.2\,mm$ polylactic acid (PLA).

complexity rises for each independent actuator. As such, independent actuator control is often sacrificed by grouping actuators and controlling them as a single unit for simplicity [7], [8].

A key factor in DMS performance is the ratio of object size to actuator pitch — the centre-to-centre spacing of adjacent actuators or the envelopes of multi-DoF actuators. Precise control becomes difficult when this ratio is low, with performance deteriorating into inoperability as objects smaller than the spacing fail to make stable contact. Consequently, most systems manipulate objects much larger than their actuator pitch, restricting the range of manipulable objects or requiring very dense actuator arrays.

While typical DMS predominantly move objects substantially larger than individual actuators, actuator-scale manipulation has also been demonstrated; such as macroscopic 3-DoF cilia actuators capable of transferring a ball between modules [6]. However, this required both high actuator density and multi-DoF motion capabilities. This illustrates the inherent trade-off between system complexity and actuator density when pursuing manipulation at this scale.

Soft connective materials have been used in DMS to provide continuous contact surfaces, which can facilitate manipulation of smaller objects—an inherent advantage of connected actuators [9], [10]. In piston-based systems, linear actuators often deform a compliant material to shape the surface. While this enables global surface control, it introduces limitations: the material must be deformable by the actuators but not deform excessively under object load. Consequently, either motors must provide high torque, objects must be light, or actuators must be densely spaced to prevent objects from resting entirely on the inter-actuator material. Ingle *et al.* [11] explored the limits of a connected piston-based DMS using a flexible, non-extensible material suspended between actuators, forming a catenary surface. Here, the material acts as the sole end effector, and object motion is governed primarily by the geometry of the suspended surface, with the pistons controlling the locations of the catenary minima. Their results demonstrate that positional control can be achieved solely through interaction with this soft material and with a significantly reduced actuator density.

Actuated surfaces with reconfigurable topologies using multiple DoF actuators have also been investigated for object manipulation [12], [13], [14]. These systems can manipulate a wide range of objects, including soft and irregular geometries. The 3-DoF actuators used have similar workspaces to our own. Our work seeks to extend these systems by significantly reducing actuator density and broadening object manipulation capabilities.

III. System Design

A. Mechanical design

The system is comprised of an array of 3-DoF parallel mechanism robotic actuators, as shown in Fig. 1. Each actuator, hereafter referred to as a *tile*, incorporates three origami-based linkages inspired by the Canfield mechanism [15], [16], [17]. Each tile features a square end effector (150×150 mm) connected to a rigid base plate via three foldable origami linkages, each inspired by a waterbomb origami fold. Each linkage is actuated by a FIT0522 geared DC motor (DFRobot).

The tiles' origami linkages follow an interpretation of a design showcased by Salerno *et al.* [12]. The linkages are created using $0.165mm$ Polyimide tape embedded within $1.2mm$ thick PLA pieces created via Fused Deposition Modelling. The polyimide is cut into a net-like pattern, shown in Fig. 1(c), using a laser cutter and embedded during the printing process by pausing fabrication to position the polyimide layer Polyimide first bonds to the PLA through its adhesive coating, but the two materials are ultimately adhered as the PLA layers fuse through channels cut into the Polyimide net, embedding it within the structure. The Polyimide is flexible, with exposed sections acting as hinges for the the origami piece.

In the modular manipulator array, individual tile modules are interconnected using flexible but effectively inextensible material, forming a continuous surface. We use a $1.5mm$ thick Linatex®natural rubber, to which a thin $0.05\,\mathrm{mm}$

polyethylene terephthalate (PET) film surface layer, used to reduce the friction between the surface and manipulated objects, is adhered using an acrylic adhesive. Given the object masses, applied motor torques, and the elastic modulus of the rubber (2 MPa), material strain during operation is negligible and the material is treated as inextensible. However, its slight compliance can prevent damage to the modules in the case of hyper-extension. The surface is attached to each tile's end effector using four recessed Velcro®hook-and-loop patches, allowing for rapid attachment and removal.

B. Electronics, Communications, and Control

The system is designed as a DMS composed of cooperating robotic tiles; consequently, modularity and distributed control were central design considerations. Each tile is equipped with an onboard Teensy ®MicroMod microcontroller responsible for end-effector position control and inter-tile communication. Each motor is controlled by a DRV8833 motor driver, which attaches to a custom-made main electronics board via a shield.

Tiles communicate locally via serial communication, allowing them to communicate with neighbouring tiles in each of their 4 cardinal directions through connectors linked to the Teensy hardware serial ports, enabling commands to be forwarded directionally or addressed using unique tile IDs.

End-effector motion is controlled using a cascaded discrete-time velocity–position PID controller, providing accurate position tracking while maintaining desired manipulation speeds.

C. System configuration

The system is a DMS, constituting an array of robotic modules connected by a soft actuated surface. In this work, we demonstrate a simple linear configuration using 3 tiles equally spaced along a singular axis, as shown in Fig. 1. The distance from tile centre to tile centre, D, dictates ranges for system parameters such as inter-tile material length, L, which in turn constricts the possible tile motions. We investigate a range of values for D and L, and their impact on achievable motions and object manipulation capabilities of the system.

IV. Kinematics and Workspaces

To analyse the motion of the connected tile array, we first characterise the kinematics and workspace of a single tile. We then examine how the connective material constrains the shared workspace of multiple tiles operating as a coupled system.

A. Kinematics

The workspace of the parallel mechanism tiles used in this work depends primarily on two geometric parameters: leg length and leg positioning. The length of the origami legs, l, used in this system is divided equally by the central waterbomb joint (ball and socket), creating the lower and the upper leg. The base of each of the origami legs is given in polar coordinates $(R, \phi_i, 0)$ with origin at the centre of the robot's base, where ϕ_i is the angle of rotation about the Z axis and R is the radius of the circle inscribed by the legs.

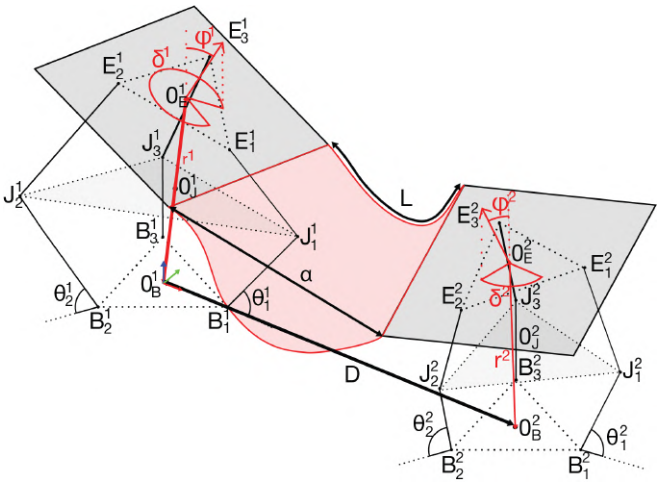

Fig. 2: Illustration of two modules modules connected by connective material. This shows motor angles θ_i, which orient the tile into a pose, (δ^i, ϕ^i, r^i). Modules are at an inter-module distance, D, and are connected by a material of length L.

In our system, leg length $l = 130\,\text{mm}$, leg positions $\Phi_1 = \frac{\pi}{3}$, $\Phi_2 = \pi$, $\Phi_3 = \frac{5\pi}{3}$, and the radius of the inscribed circle $R = 44.01\,\text{mm}$.

The kinematics for a 3-DoF Canfield parallel mechanism have been explored previously, with Mete *et al.* [18] notably deriving the end effector positions as functions of the angles between each leg and the base. Their formulation is directly applicable and is adopted here.

The kinematics of the parallel mechanism take as input the input leg angles, θ_i, and yields the position of the end-effector centre O_E relative to the base centre O_B, where we define the local coordinate frame XYZ. The relative position of O_E is expressed in polar coordinates (δ, ϕ, r), where δ is the angle of rotation about the Z axis (yaw), and ϕ is the angle of rotation about the transformed Y axis (composite pitch and roll), which determines end effector tilt. This is illustrated in Fig. 2. The value of r defined as:

$$||\overrightarrow{O_B O_E}|| = r \tag{1}$$

$$\overrightarrow{O_B O_E} = r \begin{bmatrix} \sin\phi\cos\delta \\ \sin\phi\sin\delta \\ \cos\phi \end{bmatrix} = r\vec{n} \tag{2}$$

Where $\vec{n}$ is the unit vector in the direction of $\vec{O_B O_E}$.

Due to the symmetry of the mechanism, the revolute joints connecting the origami legs to the base and to the end effector are symmetric about a virtual plane passing through the central joint of each leg. Consequently, if the positions of the central joints J_i are known, the end-effector pose can be uniquely determined. We compute the positions of J_i using the method described by Mete *et al.* [18].

B. Workspace - Single Tile

Using the forward kinematics, we map the reachable workspace for each module. The angles of the legs, θ_i, are

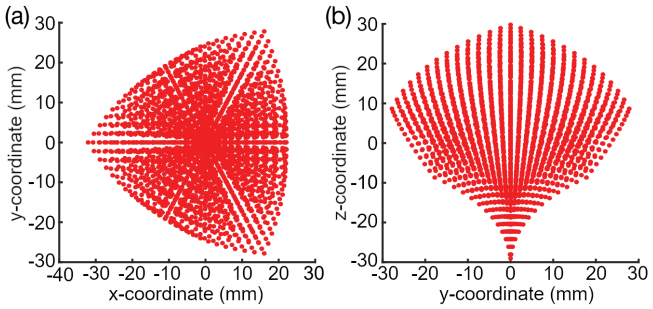

Fig. 3: Single robotic tile workspace.

constrained to the range $0 \leq \theta_i \leq \frac{7\pi}{18}$, to prevent damage to the mechanism caused by overextension.

Fig. 3 shows a visualization of a single tile's workspace, created by sweeping through the range of each leg's range and scattering the calculated end-effector position.

C. Workspace - Connected Tiles

Although each tile can independently reach any position in its workspace, this system operates as an array of actuators coupled by a shared surface. As such, we must consider if connected tiles can simultaneously reach points in their individual workspaces while connected by a length of material, L.

Given two tiles, X and Y, we define two local coordinate frames at their bases, O_B^X and O_B^Y, and at their end effectors O_E^X and O_E^Y.The relative position of the frames is determined by each tile's pose. The distance between these two tiles, D, is given by $D = ||\overrightarrow{O_B^X O_B^Y}||$.

Each tile has a square end effector with edge length E_w, and height E_h whose corners are given in a local end-effector frame by:

$$C_F = [(\frac{i \cdot E_w}{2}, \frac{j \cdot E_w}{2}, E_h)]_{O_E^F}, \quad i, j \in \{-1, 1\}, F \in \{X, Y\} \tag{3}$$

Considering the position of these corners in a shared frame, the distance between all corners for two robotic modules at any pose can then be calculated.

By transforming these corner coordinates into a shared reference frame, the pairwise distances between all corners of the two end effectors can be computed. The tiles are assumed to be connected along their closest proximal edges. The most distal corners of the closest adjoining edge are taken to be the maximum distance between the two robot end effectors. We denote this distance α, as illustrated in Fig. 2.

We may then impose a constraint $L \geq \alpha$, where L is the length of the material connecting the two tiles. Any configuration violating this constraint is considered unreachable. The shared workspace of the connected tiles is therefore defined as the set of end-effector poses that satisfy this geometric condition. This approach generalises naturally to arrays of multiple connected tiles

It should be noted that distance α measures from end-effector corner to end-effector corner, while D is given from tile centre to tile centre. This means, for a given E_w, it is possible for a configuration where $D \geq \alpha$ to be valid.

Fig. 4(a) illustrates how α varies as δ and ϕ change for two connected tiles at a fixed r_0.The plot reveals δ and ϕ have a complex, non-linear effect on α.

V. Movement Pattern Analysis

Object manipulation is achieved through coordinated tile motion. However, the interconnection of actuators means not all poses can be reached simultaneously, restricting the shared workspace and limiting feasible motions. In this section, we analyse a simple sinusoidal motion primitive and examine how system parameters, including the inter-tile distance D and connective material length L, influence achievable motions.

A. Sinusoidal Movement Pattern

For this movement pattern, δ is fixed for all tiles, aligned with the tile array, an angle we shall call Δ, where $\Delta = 0$ for the configurations studied here. The value of ϕ for each tile oscillates in the range $\phi_{max} \geq \phi \geq -\phi_{max}$, where ϕ_{max} is determined by the shared workspace constraint, discussed later. The value for a specific ϕ_i at a given time, t, is denoted ϕ_s^i:

$$\phi_i^t = \phi_{max} \sin(2\pi f_s t + p_s^i) \tag{4}$$

where f_s is the frequency of oscillation, and p_s^i is the phase offset of tile i.

A nominal base-to-end-effector distance, r_0, is selected. The distance is then optionally modulated using a second sinusoidal trajectory, r:

$$r = r_0 + h_{max} \sin(2\pi f_h t + p_h^i) \tag{5}$$

where $h_{\max}$ is the maximum height variation, f_h is the height oscillation frequency, and p_i^h is the corresponding phase offset.

Therefore, each tile tilts periodically, with optional vertical oscillation. All tiles share the same values of f_s, f_h, $\phi_{\max}$, r_0, and $h_{\max}$, but differ in the phase offsets of their sinusoidal motions. The phase difference between adjacent tiles are constants, P_s and P_h, defined by:

$$p_s^i = p_s^{i-1} + P_s \tag{6}$$

$$p_h^i = p_h^{i-1} + P_h \tag{7}$$

We impose the constraint that at $t = 0$ the first tile in the array will have $p_s = 0$, ensuring that the first tile begins in a level configuration suitable for object placement.

The pose of tile i at time t is given by:

$$\begin{bmatrix} \delta_i \\ \phi_i \\ r_i \end{bmatrix} = \begin{bmatrix} \Delta \\ \phi_{max} \sin(2\pi f_s t + P_s \times (i-1)) \\ R_0 + h_{\max} \sin(2\pi f_h t + P_h \times (i-1)) + p_h^i \end{bmatrix} \tag{8}$$

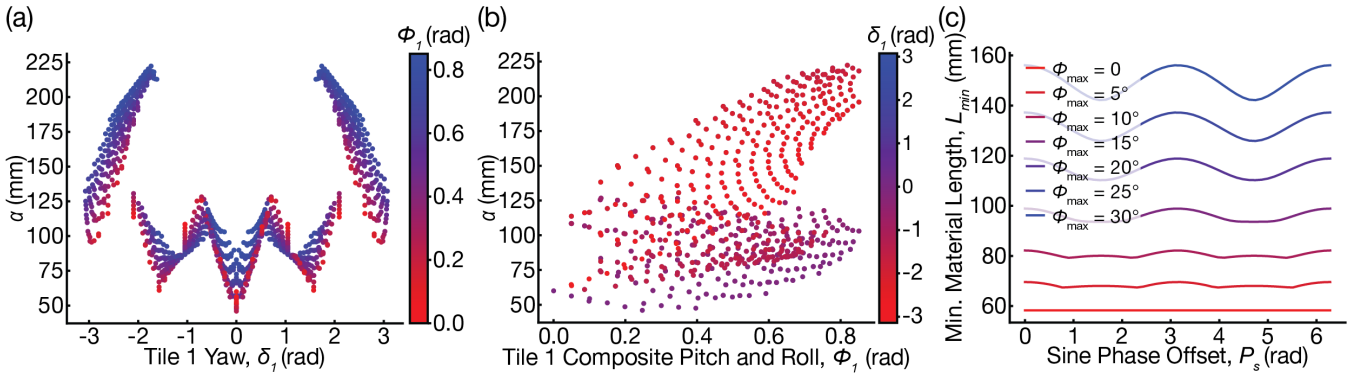

Fig. 4: Distance between connected end-effectors for static and dynamic tiles. (a, b) Variation of α between two connected tiles as Tile 1 orientation (δ_1, ϕ_1) changes, with Tile 2 fixed at $\delta_1 = 0$, $\phi_1 = 0$, $r_1 = 70\,\text{mm}$ at (210, 0, 0),mm, and Tile 1 at (0, 0, 0),mm with $r_1 = 70\,\text{mm}$. (b) Effect of phase offset P_s on minimum material length $L_{\min}$ under sinusoidal motion at different maximum tilts $\phi_{\max}$.

B. Achievable Motions

With the movement pattern defined, we now examine how system parameters D and L influence valid motion patterns, including the maximum tilt $\phi_{\max}$ and the inter-tile phase offset P_s. A motion pattern is considered feasible if, for all time steps within one cyclic period, the connectivity constraint $L \geq \alpha$ is satisfied. As tiles are connected in series, performing similar motions with a constant phase offset between neighbours, it is sufficient to evaluate the connection between two adjacent tiles to ensure compliance throughout the array. This approach allows us to determine the minimum length of connective material $L_{\min}$ required for the constraint to be valid for all time steps across the array when executing a specific motion pattern.

To study the influence of system parameters, baseline values were defined as:

$$\text{Default} = \left\{ \begin{array}{cc} O_B^1 = (0,0,0)\,\text{mm}, & O_B^2 = (400,0,0)\,\text{mm}, \\ f_s = 1\,\text{Hz}, & f_h = 1\,\text{Hz}, \\ h_{\max} = 0.0\,\text{mm}, & \phi_{\max} = \frac{\pi}{9}, \\ P_s = 0\,\text{Hz}, & P_h = 0\,\text{Hz}, \\ r_0 = 70\,\text{mm} & \end{array} \right\} \tag{9}$$

Unless otherwise stated, all subsequent analyses use these default values.

As an initial test, we investigate how L_{min} varies with changes in D. This is done by positioning the second tile at $(x, 0, 0)$ and sampling 50 evenly spaced values of x within the range $[210, 400]\,\text{mm}$. As expected, $L_{\min}$ increases linearly with inter-tile distance. Next, we investigate the effect of P_s on L_{min}. We sampled 50 values for P_s in the range $[0, 2\pi]$. The value for L_{min} varies sinusoidally with phase offset. Finally, we investigate the effect that the value for $\phi_{\max}$ has on $L_{\min}$. We sampled 50 values for $\phi_{\max}$ in the range $[0, \frac{\pi}{6}]$, from which the value of L_s was found to vary non-linearly. Fig. 4(b) shows a visualization of how L_{min} varies with changes to $\phi_{\max}$ and P_s.

VI. Object Manipulation

This section examines the system's capability to perform object manipulation, specifically linear object translation across the array.

A. Experimental Setup

Objects were placed at the centre of the left-most tile. The task was to translate objects using tile motion until they reached the edge of right-most tile, falling into a detection area, within a threshold time of 20 s. All experiments were repeated at least three times, with three consecutive successes required for a manipulation strategy to be considered successful.

Object positions were tracked with a 2-camera HSV based tracking system using the OpenCV library [19]. To facilitate robust visual detection, objects were created using a bright, mono-coloured PLA. ArUco markers fixed at known locations were used to translate pixel coordinates to real-world positions.

B. Translation Experiments - Rolling

To evaluate rolling-based manipulation, a cylinder ($\varnothing 40 \times 170$ mm) was translated, using the previously described sinusoidal motion pattern. Through systematic variation of motion parameters, two effective movement patterns were identified and experimentally validated for fixed values of inter-tile distance D and material length L.

When tiles oscillated fully in phase or completely out of phase ($P_s = 0, \pi$), translation was ineffective. Reliable translation required a phase offset of $P_s = \frac{\pi}{2}$. The frequency of the oscillation had to ensure sufficient time for the object to roll fully into the inter-tile region before the next cycle begins. Experimentally, $f_s = 0.25\,\text{Hz}$ satisfied this requirement.

Translation requires an object to move from a tile onto the inter-tile material and subsequently onto the neighbouring tile.Tilting readily moves an object onto the inter-tile material, but transferring from there to the next tile while it is in a receptive pose is more challenging. As tiles rotate about their base, not the centre of their end effector, the inter-tile material

becomes slack as tiles tilt towards each other, and becomes taut when tiles tilt away. During motion, objects often move between these areas of slack material before being ejected if the material becomes taut. Using kinematic analysis, we determine the values of ϕ and r that will ensure tautness in the material for a given tile spacing and inter-tile material length.

Height oscillations with a phase offset between neighbouring tiles create a gradient for the cylinder to roll down. These oscillations also increase end-effector separation, α, thereby pulling the inter-tile material taut.

Allowing tiles to tilt without restriction, thereby enabling a larger achievable $\phi_{\max}$, was experimentally found to improve translation. This occurs either when the phase difference P_s was near zero - though this conflicted with the directionality requirement - or when the inter-tile material length L was high relative to the inter-tile distance D. However, if L exceeded a threshold, tiles could not pull the material taut to eject objects. In all successful cases, the movement parameters pulling the inter-tile material taut was essential, making $L : D$ a critical design parameter.

Two movement patterns, denoted $\mathbf{A}$ and $\mathbf{B}$, given by:

$$\mathbf{A} = \left\{ f_s = 0.25Hz, f_h = 0.25Hz, P_s = \tfrac{\pi}{2}, P_h = \pi \right\} \quad (10)$$

$$\mathbf{B} = \left\{ f_s = 0.25Hz, f_h = 0.5Hz, P_s = \tfrac{\pi}{2}, P_h = 0 \right\} \quad (11)$$

As illustrated in Fig. 5, both patterns capture the cylinder within the inter-tile material and then eject it in the direction of translation as the material is pulled taut. Ejection occurs as the first tile tilts away, with a height offset due to P_h increasing α. The receiving tile begins tilted toward the object and levels as the object is transferred onto it.

A trade-off exists between achievable $\phi_{\max}$ and $h_{\max}$. Experimental results indicated that maximizing $h_{\max}$ was most advantageous; it was therefore set to its maximum value of $15\,\mathrm{mm}$. Subsequently, $\phi_{\max}$ was set to its upper limit as allowed by the workspace, up to a maximum of $\frac{5\pi}{36}$ - to ensure that each tile could achieve the required pose.

The calculated value of α was found to underestimate the achievable distances without causing strain in the physical system. This discrepancy arose from a combination of factors such as motor backlash, encoder resolution, and compliance in the origami components. To compensate, an additional factor of $\frac{\pi}{18}$ was added to the calculated $\psi_{\max}$ to account for the slack, but not exceeding the maximum of $\frac{25\pi}{180}$.

Table I summarises the manipulation experiments. Without a connective material ($L = 0$) we show the object was unable to translate. Introducing an interconnecting surface enabled translation across multiple inter-tile distances, including $D = 340\,\mathrm{mm}$—over twice the tile end-effector width. With an inter tile distance, D, and an end effector width, w, the effective traversable distance can be approximated by:

$$\text{Increase factor} = \frac{2D + w}{3w} \approx 1.84 \quad (12)$$

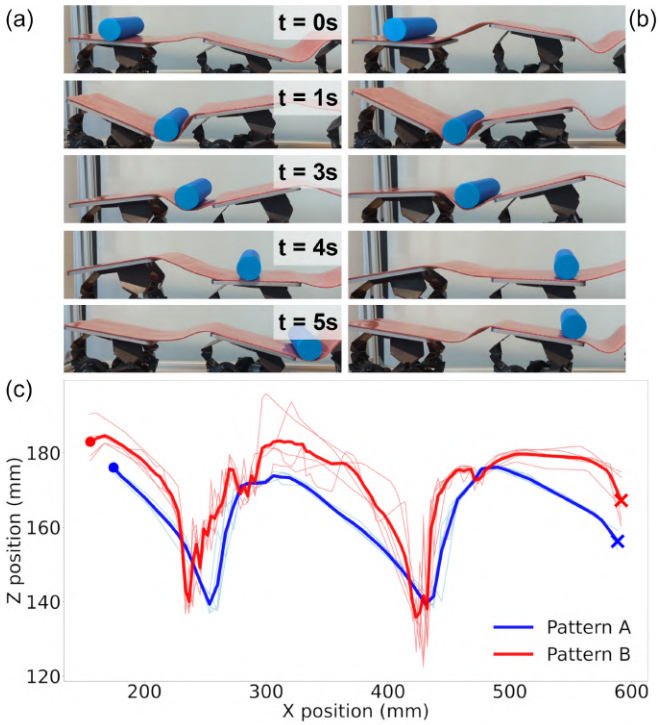

Fig. 5: Cylinder manipulation experiments. Video frames showing a cylinder manipulated using motion pattern A (a) and B (b), illustrating the similarity in object motion between the two patterns. (c) Average trajectory of the cylinder over five trials for patterns A and B with $D = 240\mathrm{mm}$ and $L = 100\mathrm{mm}$.

This corresponds to an approximate $1.84\times$ increase in traversable distance, along with a proportional decrease in actuator density relative to an equivalent densely packed system, though the true value would depend on factors such as envelope overlap. These results demonstrate the effectiveness of the inter-connective material in overcoming object-to-actuator pitch constraints, able to manipulate an object much smaller than the actuator end effectors and the inter-actuator spacing.

C. Translation Experiments - Sliding

To evaluate sliding-based manipulation, a flat circular disk ($\varnothing 60\,\mathrm{mm} \times 5\,\mathrm{mm}$) was manipulated along the array. The disk translates exclusively by sliding - as such, it required a modified manipulation strategy.

The sinusoidal motion was replaced by a six-state cyclic sequence that explicitly controls tile tilt direction and height, as defined in Table II. Tiles advance through the sequence with a dwell time of $t_s = 5\,\mathrm{s}$, as this ensures objects have sufficient time to traverse to the next part of the array. Neighbouring tiles are phase-shifted by three states. As we have 6 states, this produces an alternating pattern that promotes material capture and ejection.

Due to increased friction from the larger contact area of the disk, a vertical vibration ($5\,\mathrm{Hz}$, $5\,\mathrm{mm}$ amplitude) was applied to prevent objects stalling.

TABLE I: Results of cylinder translation experiments. Symbols: ✓ successful translation for both , ✗ failed translation, Inv invalid configuration (distance > material length), and – untested.

L (mm)									
200	-	-	-	-	-	✗	✗	✗	✓
150	-	-	✗	✗	✗	✓	Inv	Inv	Inv
100	-	✗	✓	✓	Inv	Inv	Inv	Inv	Inv
50	✗	✓	Inv	Inv	Inv	Inv	Inv	Inv	Inv
0	✗	-	-	-	-	-	-	-	-
D (mm)	180	200	220	240	260	280	300	320	340

TABLE II: State definitions for sliding object translation sequence. Φ_F and Φ_B denote a specific forward and backward tilt angle, while R_H and R_L are set high and low tile heights.

State	δ	ϕ	r_0
1	0	Φ_F	R_H
2	π	Φ_B	R_H
3	–	0	R_H
4	π	Φ_B	R_L
5	–	0	R_L
6	0	Φ_F	R_H

By cycling these states, both objects were manipulated across the arrays with an inter-tile distance of 240, 280, and 340mm, with inter-tile material lengths of 100, 150, and 200mm respectively. The values of the parameters, Φ_F, Φ_B, R_H, and R_L were selected to ensure material tautness for each configuration using calculation of α. The specific values are detailed in Table III. Greater tile spacing required tiles to tilt further or have a greater difference in height between their high and low states to ensure that the inter-tile material was pulled taut and that a significant gradient was maintained when traversing the longer connective material between tiles.

D. Translation Experiments - Sliding and Rolling

Finally, we repeated the translation experiments with a cube ($40\,\mathrm{mm}^3$). The cube alternates between rolling and sliding depending on its orientation relative to the surface during actuation.

Using the same cycling movement pattern used for the disk, we were successful at translating the object across the same inter tile distances, using the same length of material, and movement parameters. However, successful translation of the cube was highly dependent on initial positioning. Transitioning between sliding and rolling occasionally caused unpredictable movement, resulting in semi-chaotic motion and occasional failures in translation, highlighting the limitations of open-loop manipulation for mixed-mode object dynamics.

VII. Discussion

The proposed system combines 3-DoF robotic tiles with a compliant inter-tile material, forming a hybrid soft–rigid

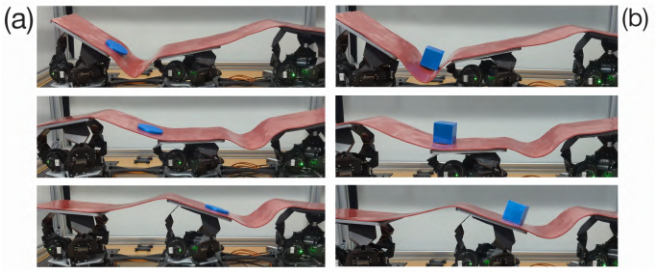

Fig. 6: Video frames of the first 3 cycles of manipulation experiments. (a) Manipulating the disk (b) Manipulating the cube

TABLE III: Successful manipulation parameters for state translation of non-cylindrical objects for different material lengths (L) and inter-tile spacings (D)

L:D(mm)	Φ_F	Φ_B	R_H (mm)	R_L (mm)
100:240	$\frac{5\pi}{36}$	$\frac{\pi}{12}$	70	40
150:280	$\frac{\pi}{6}$	$\frac{\pi}{12}$	80	40
200:320	$\frac{5\pi}{36}$	$\frac{\pi}{12}$	85	40

distributed manipulation surface. Rigid linkages and flat end-effectors provide predictable actuator kinematics and well defined manipulation on top of end-effectors, while the compliant surface layer ensures continuous object contact across tile boundaries, eliminating the discrete contact discontinuities inherent to non-connected tiles.

In this work, we demonstrated object translation using a linear actuator array. A natural extension is to employ a two-dimensional DMS array, facilitating richer manipulation tasks including planar transport and rotation.. This is an avenue we will explore in future work. However, computing the valid workspace using the motion of only two connected tiles would not hold when tiles are interconnected in multiple dimensions. Similarly, non-periodic motion patterns would significantly increase the computational complexity of workspace validation, motivating the need for more efficient constraint-checking or online planning methods.

We demonstrated translation using simple geometric objects. While this serves as a proof-of-concept, objects of other geometries may follow different trajectories and require modified movement patterns for reliable translation. Irregular geometries may also move in a less predictable manner, necessitating novel manipulation strategies. Although our focus is on objects smaller than the inter-actuator spacing, larger objects that contact multiple tiles simultaneously would require different manipulation strategies, such as gating. We would also like to investigate the manipulation of deformable objects, for which the absence of grasping may be advantageous.

All experiments employed open-loop, hand-crafted manipulation strategies to demonstrate the system's functionality and the role of the connective material. Future work should explore closed-loop control and manipulation strategies for

greater manipulation precision, enabling targeted motions based on object location and allowing selective application of movements such as vibration when an object becomes stuck.

The inter-tile material plays a central role in enabling low actuator density. In this work, we consider the material as inextensible. This is not true of real-world materials; though this approximation holds for the object masses and motor torques tested. In the real world, compliance may cause hysteresis and energy loss, potentially reducing manipulation precision and repeatability. Future work should examine how material stretch affects object manipulation, reachable workspaces, positional drift over cycles, and motor loading, as well as exploring ways to exploit or mitigate this behaviour.

The high coefficient of friction of the inter-tile material required the use of vibration to mobilize objects that would otherwise remain stationary. However, preliminary trials with lower-friction materials while facilitating motion, also led to uncontrolled sliding, diminished repeatability, particularly in open-loop operation. Future work will investigate intermediate or tunable friction materials, as well as control strategies that explicitly account for frictional effects, to improve robustness and precision in object manipulation.

VIII. Conclusion

This work introduces a soft, interconnected actuator array that enables effective object manipulation with significantly reduced actuator density. By interconnecting actuators with a flexible material the proposed design not only extends the reachable workspace but also relaxes traditional scale and density constraints inherent to distributed manipulator systems. Through kinematic analysis and the implementation of sinusoidal and cycling state based movement patterns, the system successfully translated objects of different geometries across a large distance, achieving a $1.84\times$ increase in .traversable distance when compared to a similar, densely packed system that did not use connective material.

IX. Acknowledgments

This work was conducted as part of the MOZART project, funded by the European Union, EU project id: 101069536.

References

[1] Z. Xue, H. Zhang, J. Cheng, Z. He, Y. Ju, C. Lin, G. Zhang, and H. Xu, "ArrayBot: Reinforcement Learning for Generalizable Distributed Manipulation through Touch," Jun. 2023.

[2] D. Parajuli, M. D. Bedillion, and R. C. Hoover, "Actuator Array Manipulation Using Low Resolution Local Sensing," in *ASME 2014 International Mechanical Engineering Congress and Exposition*. American Society of Mechanical Engineers Digital Collection, 2014.

[3] T. D. Murphey and J. W. Burdick, "Feedback Control Methods for Distributed Manipulation Systems that Involve Mechanical Contacts," *The International Journal of Robotics Research*, vol. 23, no. 7-8, pp. 763–781, Aug. 2004.

[4] S. Thompson, P. Mannam, Z. Temel, and O. Kroemer, "Towards Robust Planar Translations using Delta-manipulator Arrays," in *2021 IEEE International Conference on Robotics and Automation (ICRA)*. Xi'an, China: IEEE, May 2021, pp. 6563–6569.

[5] S. Patil, T. Tao, T. Hellebrekers, O. Kroemer, and F. Z. Temel, "Linear Delta Arrays for Compliant Dexterous Distributed Manipulation," in *2023 IEEE International Conference on Robotics and Automation (ICRA)*, May 2023, pp. 10 324–10 330.

[6] M. Yim, J. Reich, and A. A. Berlin, "Two Approaches to Distributed Manipulation," in *Distributed Manipulation*, K. F. Böhringer and H. Choset, Eds. Boston, MA: Springer US, 2000, pp. 237–261.

[7] K.-F. Bohringer, V. Bhatt, and K. Goldberg, "Sensorless manipulation using transverse vibrations of a plate," in *Proceedings of 1995 IEEE International Conference on Robotics and Automation*, vol. 2, May 1995, pp. 1989–1996 vol.2.

[8] M. Ataka, B. Legrand, L. Buchaillot, D. Collard, and H. Fujita, "Design, Fabrication, and Operation of Two-Dimensional Conveyance System With Ciliary Actuator Arrays," *IEEE/ASME Transactions on Mechatronics*, vol. 14, no. 1, pp. 119–125, Feb. 2009.

[9] GB. Festo, "WaveHandling," https://www.festo.com/gb/en/e/about-festo/research-and-development/bionic-learning-network/highlights-from-2013-to-2014/wavehandling-id_33578/, 2013.

[10] R. Hashem, B. Smith, D. Browne, W. Xu, and M. Stommel, "Control of a soft-bodied XY peristaltic table for delicate sorting," in *2016 IEEE 14th International Workshop on Advanced Motion Control (AMC)*. Auckland, New Zealand: IEEE, Apr. 2016, pp. 358–363.

[11] P. Ingle, K. Støy, and A. Faiña, "Soft Manipulation Surface With Reduced Actuator Density For Heterogeneous Object Manipulation," Nov. 2024.

[12] M. Salerno, J. Paik, and S. Mintchev, "Ori-Pixel, a Multi-DoFs Origami Pixel for Modular Reconfigurable Surfaces," *IEEE Robotics and Automation Letters*, vol. 5, no. 4, pp. 6988–6995, Oct. 2020.

[13] Z. Wang, S. Demirtas, F. Zuliani, and J. Paik, "Surface-based manipulation with modular foldable robots," *npj Robotics*, vol. 4, no. 1, p. 3, Jan. 2026.

[14] Y. Jiang, S. E. Asmar, Z. Wang, S. Demirtas, and J. Paik, "CPG-Based Manipulation with Multi-Module Origami Robot Surface," Feb. 2025.

[15] S. L. Canfield, "Development of the Carpal Wrist; a Symmetric, Parallel-Architecture Robotic Wrist," May 1997.

[16] K. Zhang, C. Qiu, and J. S. Dai, "An Extensible Continuum Robot With Integrated Origami Parallel Modules," *Journal of Mechanisms and Robotics*, vol. 8, no. 031010, Mar. 2016.

[17] M. Salerno, K. Zhang, A. Menciassi, and J. S. Dai, "A Novel 4-DOF Origami Grasper With an SMA-Actuation System for Minimally Invasive Surgery," *IEEE Transactions on Robotics*, vol. 32, no. 3, pp. 484–498, Jun. 2016.

[18] M. Mete and J. Paik, "Closed-Loop Position Control of a Self-Sensing 3-DoF Origami Module With Pneumatic Actuators," *IEEE Robotics and Automation Letters*, vol. 6, no. 4, pp. 8213–8220, Oct. 2021.

[19] G. Bradski, *The Opencv Library*, Nov. 2000, vol. 25.